https://doi.org/10.5194/egusphere-2026-3019
Preprint. Discussion started: 11 June 2026

Plutonium isotopes as time-markers in South American lake sediments: identifying pre- and post-1959 and French test periods

Floriane Guillevic[1*], Renaldo Gastineau[2,3], Olivier Evrard[4], Pierre Sabatier[3], Amaury Bardelle[4], Pierre-Alexis Chaboche[4], Anthony Foucher[4], Romina Achaga[5], Ana Carolina Ruiz-Fernández[6], Joan-Albert Sanchez-Cabeza[6], Marcos Tassano[7], Mirel Cabrera[7], Juan A. Quicke[8], Guillermo Chalar[9], Maarten Van Daele[10], Valentina Moreno-Allende[11], Jasper Moernaut[11], Torsten Haberzettl[12], José A. Corcho Alvarado[13], Stefan Röllin[13], Hans Sahli[13], Judith Kobler[1], Gerald Dicen[1], Christine Alewell[1]

[1]Environmental Geosciences, University of Basel, Basel, CH-4056, Switzerland
[2]International Research Institute of Disaster Science, Tohoku University, 468-1, Aoba, Aramaki, Aoba-ku, Sendai, Miyagi, 980-8572, Japan
[3]EDYTEM, Université Savoie Mont-Blanc, CNRS, 73376, Le Bourget du Lac, France
[4]Laboratoire des Sciences du Climat et de l'Environnement (LSCE), CEA, CNRS, UVSQ, Université Paris-Saclay, Gif-sur-Yvette 91198, France
[5]Centro de Investigaciones en Física e Ingeniería Del Centro de La Provincia de Buenos Aires (CIFICEN), Universidad Nacional Del Centro de La Pcia. de Bs. As. (UNCPBA), Tandil, Argentina
[6]Unidad Académica Mazatlán, Instituto de Ciencias del Mar y Limnología, Universidad Nacional Autónoma de México, 82040, Mazatlán, Sinaloa, México
[7]Laboratorio de Radioquímica, Área de Radiofarmacia, Centro de Investigaciones Nucleares, Facultad de Ciencias, Universidad de la República, Mataojo 2055, Uruguay
[8]Instituto Nacional de Investigación Agropecuaria (INIA), Ruta 50 Km. 11, Colonia, Uruguay
[9]Sección Limnología, Facultad de Ciencias, Instituto de Ecología y Ciencias Ambientales, Facultad de Ciencias, Universidad de la República, Montevideo, Uruguay
[10]Renard Centre of Marine Geology, Department of Geology, Ghent University, Ghent, Belgium
[11]Institute of Geology, University of Innsbruck, Innsbruck, Austria
[12]Physical Geography, Institute for Geography and Geology, University of Greifswald, Greifswald, Germany
[13]Spiez Laboratory, Federal Office for Civil Protection, Spiez, Switzerland

Correspondence to: Floriane Guillevic floriane.guillevic@unibas.ch

https://doi.org/10.5194/egusphere-2026-3019
Preprint. Discussion started: 11 June 2026

Abstract. In regions where rapid and extensive environmental changes have occurred, particularly in South America, reliable time markers are essential for dating sediment sequences and quantifying environmental degradation. In this respect, the use of ^{239}Pu and ^{240}Pu isotopes in South American sediments may help to identify distinct sources of fallout radionuclides, including radioactive fallout from French atmospheric nuclear weapons tests (NWTs) conducted between 1966 and 1974 at the Mururoa and Fangataufa atolls (French Polynesia). Here, we present post-1900 continuous records of ^{240}Pu/^{239}Pu isotope ratios in sediments cores from sites located between 32° and 52°S latitude: Lakes Natri and Laja in Chile; Lakes La Barrancosa, Melincué, Ñe Luan, and Roca in Argentina; and the Rincón del Bonete Reservoir and La Estanzuela Pond in Uruguay. Depth profiles revealed two $^{240+239}$Pu activity peaks, from which the more recent is not concomitant to the ^{137}Cs maximum activity peak dated back to 1964-1965. The low ^{240}Pu/^{239}Pu atom ratio (< 0.08) associated with this more recent Pu peak confirms a contribution from French fallout, dated to the late 1960s to early 1970s. The investigated lakes exhibited similar patterns in Pu isotope ratios: (i) an initial phase dominated by the U.S. NWTs signature (^{240}Pu/^{239}Pu > 0.20, also often referred to pre-moratorium), followed by (ii) increasing Pu activities characterized by a Pu isotopic signature consistent with global fallout (^{240}Pu/^{239}Pu ~ 0.18) and, finally, (iii) a period of increased Pu activities from French NWTs fallout (0.03 < ^{240}Pu/^{239}Pu < 0.08). The ^{239}Pu and ^{240}Pu isotopes revealed a consistent nuclear source pattern with a distinct French fallout contribution, confirming their suitability as an additional time marker for environmental reconstruction in South America.

https://doi.org/10.5194/egusphere-2026-3019
Preprint. Discussion started: 11 June 2026

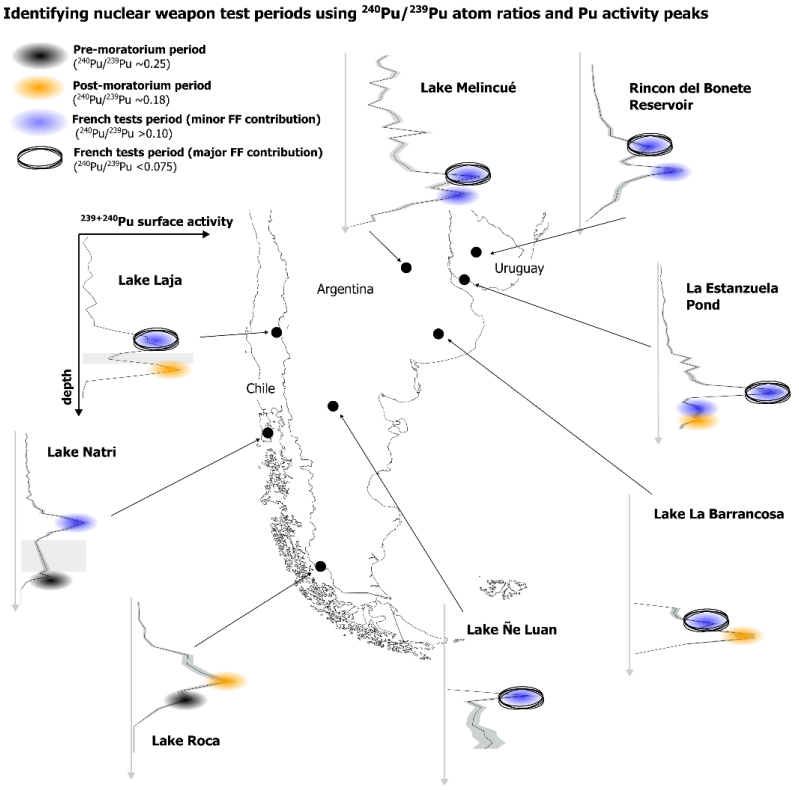

1 Introduction

Over the last century, South America has undergone rapid land-use changes and major environmental degradation, including soil erosion and contaminant releases into freshwater bodies (Zalles et al., 2021; Foucher et al., 2023; Bardelle et al., 2025). However, uncertainties in the dating of environmental archives often prevent the precise reconstruction of environmental changes during the Anthropocene.

While ^{137}Cs remains widely used to validate ^{210}Pb chronologies, its application in the Southern Hemisphere (SH) has become increasingly difficult due to low fallout activities combined with its relatively short half-life ($t_{1/2}$ = 30.02 a; Mougeot et al., 2025). As most nuclear tests were conducted in the Northern Hemisphere (NH) (UNSCEAR, 2000), ^{137}Cs activities in the environment often approach detection limits in the SH (Foucher et al., 2021; Guillevic et al., 2026) and require the use of ultralow background facilities (Reyss et al., 1995) that are not widely available. Moreover, the broad shape of the ^{137}Cs fallout peak typically observed in environmental records, such as in sediment cores (Barra et al., 2001; Hancock et al., 2011), often prevents a precise identification of the year of maximum radioactive fallout.

Four decades ago, Koide et al. (1985) proposed the use of plutonium isotopes (^{239}Pu, $t_{1/2}$ = 24 110 a; Browne, 2003; ^{240}Pu, $t_{1/2}$ = 6561 a, Browne and Tuli, 2006) as geochronological tools by showing that distinct ^{240}Pu/^{239}Pu atom ratios

https://doi.org/10.5194/egusphere-2026-3019
Preprint. Discussion started: 11 June 2026

are associated with different nuclear weapon sources and, consequently, with different deposition periods. Two main time periods were identified in Antarctica based on $^{240}Pu/^{239}Pu$ atom ratios in environmental archives (Buesseler, 1997; Koide et al., 1985). During the pre-moratorium period (1951-1958), the $^{240}Pu/^{239}Pu$ atom ratio was the highest (0.34-0.28), reflecting the predominance of U.S NWTs from the Pacific Proving Grounds (Enewetak and Bikini, **Fig.1**). Elevated ratios are generally expected from high-yield tests, as higher neutron fluxes produce a greater proportion of ^{240}Pu through neutron capture, though this can vary depending on weapons design (Buesseler, 1997; Ketterer and Szechenyi, 2008). The $^{240}Pu/^{239}Pu$ atom ratio declined to 0.22 just before the moratorium period, as contribution from the Soviet NWTs increased. The moratorium on nuclear testing was an agreement between the U.S, the former Soviet Union, and the United Kingdom which temporarily halted NWTs between November 1958 and September 1961. Following the moratorium period, the post-moratorium period (1961-1963) is then characterized by the large contribution of high-yield Soviet tests, resulting in a global fallout signature of 0.18 ± 0.01 (Kelley et al., 1999; Krey et al., 1976). This period is associated with the largest deposition of fallout radionuclides, dated to 1964-1965 in the SH (Bruel and Sabatier, 2020; Foucher et al., 2021; Guevara et al., 2003). Additionally to the $^{240}Pu/^{239}Pu$ atom ratio, the $^{137}Cs/^{239+240}Pu$ activity ratio have been used to distinguish sources and thereby differentiate between the pre-moratorium ($^{137}Cs/^{239+240}Pu \sim 20$, decay-corrected to 2025) to the post-moratorium period ($^{137}Cs/^{239+240}Pu \sim 10$) (Dicen et al., 2024; Hancock et al., 2011).

A third period is associated with the French NWTs after the Partial Nuclear Test Ban Treaty was signed in 1963. During this period, only France and China continued to test atmospheric nuclear weapons, with the French tests being detected in the SH (e.g. Chile and Argentina, Kelley et al., 1999; French Polynesian atolls, Bouisset et al., 2018). French tests were conducted on two atolls in French Polynesia (Mururoa and Fangataufa) between 1966 and 1974 and produced a distinct low $^{240}Pu/^{239}Pu$ atom ratio of 0.035 ± 0.015 (Bouisset et al., 2021; Chiappini et al., 1996, 1999; Hrnecek et al., 2005). Although French high-yield tests (>1 Mt) would typically suggest a higher $^{240}Pu/^{239}Pu$ atom ratio, the observed ratio remains low. This is attributed to the nuclear device design, which limited neutron absorption and thus reduced ^{240}Pu production and fission byproducts (Buesseler, 1997; Hancock et al., 2014). In South American soils, this additional input of Pu led to deviations from the global fallout signature, ranging from minor to major (Dicen et al., 2024; Kelley et al., 1999; Krey et al., 1976). Discrete sediment layers in South American lakes also showed a mix of Pu from global fallout (GF) and French fallout (FF) during the French NWTs period (Chaboche et al., 2022).

While the contribution of FF in South America is partly known (Chaboche et al., 2022; Kelley et al., 1999; Krey et al., 1976), the chronology of its deposition remains less constrained. With an ascertained fallout chronology in lake sediments, the distinct low $^{240}Pu/^{239}Pu$ atom ratio of the FF could therefore provide additional time markers for historical reconstructions. Previous results (Chaboche et al., 2022; Dicen et al., 2024) indicate ratios that are lower than those of global fallout, especially in the 30-40°S latitudinal band, including Chile and Argentina, where the contribution of the FF to total fallout was potentially the highest. However, a study conducting such measurements along a continental transect is currently lacking to confirm these observations.

Here, we investigated sediments collected from eight lakes located between 32 and 52°S latitudes (Lakes Natri and Laja in Chile; La Barrancosa, Melincué, Ñe Luan, and Roca in Argentina; and the Rincón del Bonete Reservoir and

https://doi.org/10.5194/egusphere-2026-3019
Preprint. Discussion started: 11 June 2026

La Estanzuela Pond in Uruguay). We used ^{210}Pb and ^{137}Cs short-lived radionuclides to establish sediment chronologies and ^{239}Pu and ^{240}Pu isotopic analyses to identify nuclear source fallout history. This work addresses three main questions: (1) can the history of nuclear bomb testing be reconstructed from sediment records in South America? (2) can the contribution of French nuclear tests be identified in lake sediments and used as a temporal marker? and (3) what are the relative proportions of the French nuclear tests compared to the overall fallout from Soviet and U.S. tests carried out in the Northern Hemisphere and transferred in the Southern Hemisphere?

2 Material and Methods

2.1 Study sites

The South American continent is the mainland that is located the closest to the Mururoa and Fangataufa atolls (22°S, 139°W, **Fig. 1**), in the direction of prevailing westerly winds (30°- 60°S). During the French NWTs period, tests were primarily conducted during austral winter (May-October) at these atolls, when the South Pacific Convergence Zone (SPCZ) shifts northward and envelops the atolls (Rougerie and Rancher, 1994; Ministère de la défense, 2006). Behind the SPCZ, air masses at low altitudes split into two branches: one flows westward in the direction of the southern flank of the Easter Island anticyclone, while the other circulates around the Kermadec anticyclone, gradually turning northwestward and converging with the easterly trade winds. At higher altitudes, strong westerly jet-streams winds predominate, directing toward South America. This seasonal change results in prevailing westerly winds at both surface and higher altitudes, which were intended to minimize the deposition of fallout over populated French Polynesian islands located to the northwest (Ministère de la défense, 2006).

Eight lakes were selected along west-east and north-south transects across Chile, Argentina and Uruguay in the 30-50°S latitudinal band (**Fig. 1**), where previous studies have provided evidence of a higher FF contribution in soil profiles at reference sites from these regions (Chaboche et al., 2022; Chamizo et al., 2011; Kelley et al., 1999; Salmani-Ghabeshi et al., 2018): Lake Natri (**NAT**, 42°S, 73°W) and Lake Laja (**LAJA**, 37°S, 71°W) in Chile; Lake La Barrancosa (**BAR**, 37°S, 60°W), Lake Melincué (**MEL**, 33°S, 61°W), Lake Ñe Luan (**NLU**, 41°S, 68°W) and Lake Roca (**ROCA**, 51°S, 73°W) in Argentina; and the Rincón del Bonete Reservoir (**RDB**, 32°S, 56°W) and La Estanzuela Pond (**EST**, 34°S, 57°W) in Uruguay (**Text S1**). These sites cover a range of diverse climatic zones, bioregions (**Fig S1**), lake sizes, and watershed surface areas (**Table S1**).

https://doi.org/10.5194/egusphere-2026-3019
Preprint. Discussion started: 11 June 2026

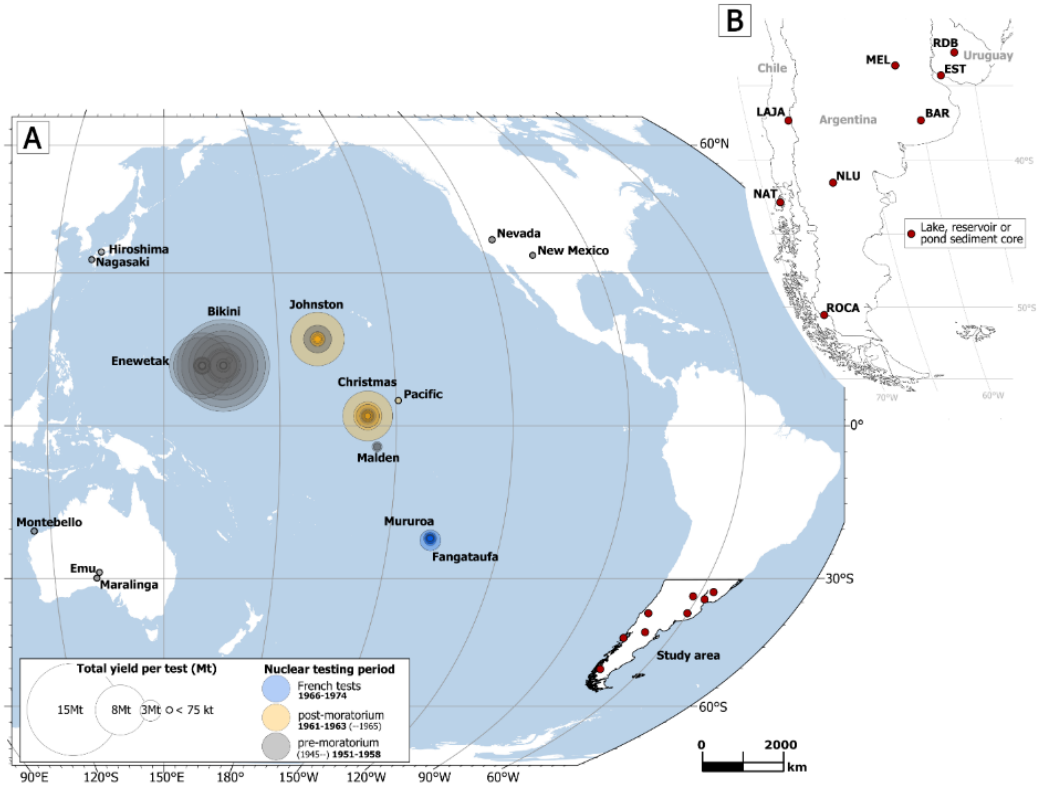

Figure 1: A) Atmospheric nuclear weapon test sites in the Pacific and surrounding continental areas, with total yield per test (UNSCEAR, 2000); B) Map of the eight studied water bodies in southern South America: Rincón del Bonete Reservoir (RDB), La Estanzuela Pond (EST), Lake Melincué (MEL), Lake La Barrancosa (BAR), Lake Ñe Luan (NLU), Lake Roca (ROCA), Lake Laja (LAJA) and Lake Natri (NAT).

2.2 Lake sampling and sediment dating

All lakes were sampled over the past five years, except **ROCA** that was sampled in 2006, and **LAJA** in 2011 (**Table S1**). A gravity corer was used to collect the sediments. This coring method ensures that the water-sediment interface remains mostly undisturbed and, above all, that no sediment is lost at this interface, thus ensuring the continuity of radionuclide measurements over the last century.

Sediment cores were subsampled continuously at a resolution of 0.5 to 2 cm, adapted to facies boundaries, to achieve an optimal temporal resolution and sufficient sample mass (**Table S1**). The sediment samples were freeze-dried or dried between 40 and 60°C for ~48 h and gently crushed using an agate mortar. Dry bulk density (DBD) was determined by measuring the dry weight of the known sampling volume (e.g. small cylinder) of sediment to allow

https://doi.org/10.5194/egusphere-2026-3019
Preprint. Discussion started: 11 June 2026

$^{239+240}$Pu and ^{137}Cs surface activities (Bq·m^{-2}) and Pu fluxes calculation (Bq·m^{-2}.yr^{-1}). After airtight tube conditioning for radionuclide measurements, a three-week delay before analysis was necessary to allow ^{222}Rn and its progeny (including ^{214}Bi and ^{214}Pb) to reach radioactive equilibrium with ^{226}Ra.

The samples were analyzed for ^{210}Pb,^{226}Ra (via ^{214}Bi and ^{214}Pb),^{137}Cs, and ^{241}Am via their gamma emissions at the Modane Underground Laboratory (France) using EDYTEM/LSCE-operated low background SAGe™ well detectors (Small Anode Germanium Detector, Mirion) or 'well' type HPGe detector (Hyper Pure Germanium, Canberra/Ortec) which allow for very low background and high counting efficiency (Reyss et al., 1995). To achieve a statistical error of less than 10% for $^{210}Pb_{ex}$ and ^{137}Cs activities, an average counting time of 24 h was necessary. The excess ^{210}Pb ($^{210}Pb_{ex}$, unsupported) activities were calculated for each sample as the difference between the total ^{210}Pb and ^{226}Ra (assumed to be in secular equilibrium with supported ^{210}Pb) activities (Bruel and Sabatier, 2020). Sediment cores from lakes Melincué and La Barrancosa had previously been analyzed in the Servicio Académico de Fechado, at Universidad Nacional Autónoma de México (Mexico) using a similar procedure. Dating results were published by Achaga et al. (2022) for Lake Melincué and Achaga et al. (2026, *submitted, 1st revision*) for Lake La Barrancosa. A few additional samples from Lake Melincué were measured at the Modane Underground Laboratory to detail the previously published ^{137}Cs downcore profile. Samples from La Estanzuela Pond were measured at the Laboratorio de Radioquímica, Centro de Investigaciones Nucleares, Facultad de Ciencias, Universidad de la República (Uruguay) following the same protocol.

Age-depth profiles were constructed using the R package serac (Bruel and Sabatier, 2020), providing an estimate of sediment deposition rate using either the Constant Flux - Constant Sedimentation rate (CFCS) or the Constant Rate of Supply (CRS) (Appleby and Oldfield, 1978) age-depth model in R software (R Core Team, 2022). To validate each model, the artificial radionuclides ^{137}Cs and ^{241}Am activity peaks were used as time-markers for the years of maximum fallout deposition, corresponding to 1964-1965 in the Southern Hemisphere (Bruel and Sabatier, 2020; Foucher et al., 2021; Guevara et al., 2003) and confirmed by air filter measurements in Buenos Aires (**Fig. S2**, Tassano et al., 2025).

2.3 Plutonium isotope analyses

The sediment samples were ashed at 600 °C for 16 h to remove organic matter. Based on available material and ^{137}Cs activity levels, acid leaching or fusion digestion was used to extract plutonium isotopes from the ashed sediments (**Fig. S3**). The acid leaching method was used at the University of Basel (Switzerland) when the sample weight was greater than 2 g. For sediment samples weighing around 2 g or less, total fusion digestion using lithium borate was undertaken at the Spiez Laboratory (Federal Office for Civil Protection, Switzerland, **Table S2**). In both methods, the ashed samples were spiked with a known amount of ^{242}Pu solution (~10 pg, traceable to NIST 4334I) prior to Pu extraction, in order to determine the radiochemical yield.

For the acid leaching method, the ashed sediments were mixed with concentrated nitric acid (HNO_3 69%, ~10mL) at a solution:sample ratio varying between 5 and 10, and heated at 80 °C overnight. Once cooled, sample solutions were diluted with 15 mL of ultrapure deionized water, mixed and centrifuged to retain only the supernatant. To convert Pu(III) into Pu(IV), sodium nitrite solution (20% $NaNO_2$) was added and heated at 70 °C for 2 h (Ketterer et al., 2004).

https://doi.org/10.5194/egusphere-2026-3019
Preprint. Discussion started: 11 June 2026

To separate Pu from other radionuclides that could interfere during measurement (e.g. U and Th), the sample solution (around 25 mL) was poured onto a pre-conditioned (2 M HNO_3) TEVA column (Tetravalent Aliphatic Quaternary Amine, Triskem). The column was washed with 2 M HNO_3 and 8 M HCl to remove U and Th, respectively. The plutonium isotopes were eluted from the TEVA columns using a diluted acid solution (0.5 M HCl). Reference soils and sediments, as well as blank samples were analyzed with each sequence of samples for quality assurance (QA) and quality control (QC). For the fusion digestion, lithium borate fusion and subsequent plutonium separation were performed according to a previously published method (Röllin et al., 2009; Sahli et al., 2017; Röllin et al., 2022). All Pu fractions were analyzed by SF-ICP-MS and MC-ICP-MS following previously published procedures (Röllin et al., 2009; Sahli et al., 2017; Röllin et al., 2022).

2.4 Plutonium-based calculation

All Pu concentrations (fg.g^{-1}) are expressed as $^{239+240}$Pu activity concentration (Bq·kg^{-1}) or as $^{239+240}$Pu surface activity (Bq·m^{-2}) to account for changes in dry bulk density (DBD, g.cm^{-3}) along sediment cores using:

$$^{239+240}Pu_{surface\ activity} = A * DBD * D \quad (1)$$

where A (Bq·kg^{-1}) is the $^{239+240}$Pu activity concentration of the sample and D (cm) is the thickness of layer. The same equation was used to calculate ^{137}Cs surface activity replacing $^{239+240}$Pu activity concentration by ^{137}Cs surface activity. To compare plutonium deposition among lakes over time, $^{239+240}$Pu flux was calculated for each sample using:

$$Pu_{flux} = A * DBD * SR \quad (2)$$

where Pu_{flux} is the flux of $^{239+240}$Pu (Bq·m^{-2}·yr^{-1}), A (Bq·kg^{-1}) is the $^{239+240}$Pu activity concentration of the sample and SR (cm·yr^{-1}) is the sedimentation rate, established from the $^{210}Pb_{ex}$ chronology. Inventories were calculated to compare total Pu deposition among lakes as well as with atmospheric deposition, using:

$$I_{total} = \sum_{i=0}^{n} A_i \times DBD_i \times D_i \quad (3)$$

where I_{total} (Bq·m^{-2}) is the total inventory, i is the sampling layer sequence, n is the sampling layer, D_i (cm) is the thickness of layer i, and A_i (Bq·kg^{-1}) is the Pu activity concentration for each layer. We defined I_{peak} (Bq·m^{-2}) as the partial inventory representing Pu deposition during the nuclear weapons testing period, restricted by the endpoint depths of the $^{239+240}$Pu and ^{137}Cs peaks. DBD was measured for all samples, whereas Pu measurements were sometimes discontinuous and were linearly interpolated between samples using the *na.approx* function from the *zoo* R package (Zeileis and Grothendieck, 2005). These inventories were compared with latitudinal band reference inventories based on reference soil sites from the literature (Dicen et al., 2024), as well as with the soil reference inventory collected near La Estanzuela Pond (I_{EST} = 22.5 ± 0.8 Bq·m^{-2}), consistent with values reported for the 30-40° latitudinal band (**Table 1**).

To quantify the relative contribution of FF and GF to Pu deposition in lake sediments, we applied a simple un-mixing model based on the distinct ^{240}Pu/^{239}Pu isotopic signature of each source. Atmospheric nuclear tests conducted during

https://doi.org/10.5194/egusphere-2026-3019
Preprint. Discussion started: 11 June 2026

the post-moratorium period produced fallout that peaked in the SH in the mid-1960s (1964-1965) and defined the GF $^{240}Pu/^{239}Pu$ isotopic signature of 0.18 ± 0.01 (Kelley et al., 1999; Krey et al., 1976).

In contrast, the FF signature is characterized by a low $^{240}Pu/^{239}Pu$ atom ratio of 0.035 ± 0.015 (Bouisset et al., 2021; Chaboche et al., 2022; Chiappini et al., 1996). However, this FF signature range may not fully represent all French NWTs, as these ratios are derived from material collected on the atolls and do not account for high-yield thermonuclear tests, whose fallout primarily released into the stratosphere remains unpublished.

Pre-moratorium tests were not included in the FF fraction calculation, as their fallout were not concurrent with the French testing period, and their contribution to the total Pu inventory is considered minor relative to GF. This assumption is supported by the GF $^{240}Pu/^{239}Pu$ isotopic signature measured in stratospheric air samples from 1966 and 1967 (Leifer and Chan, 1997). British tests conducted in Australia approximately ten years prior to the French tests were also excluded due to their low yield and predominantly regional fallout deposition (Child and Hotchkis, 2013; Dicen et al., 2024) likely not reaching South America. The fraction of Pu derived from the French tests ($FF_{fraction}$) was calculated using:

$$FF_{fraction} = \frac{\frac{240Pu}{239Pu}_{GF} - \frac{240Pu}{239Pu}_{i}}{\frac{240Pu}{239Pu}_{GF} - \frac{240Pu}{239Pu}_{FF}} \quad (4)$$

where i is the sampling layer. The global fallout fraction ($GF_{fraction}$) was then determined as:

$$GF_{fraction} = 1 - FF_{fraction} \quad (5)$$

Uncertainties were propagated using the *error* R package. The uncertainty in the Pu_{flux} ($u(Pu_{flux})$) was calculated for each layer as:

$$u(Pu_{flux}) = Pu_{flux} \times \sqrt{\left(\frac{u(A)}{A}\right)^2 + \left(\frac{u(DBD)}{DBD}\right)^2 + \left(\frac{u(SR)}{SR}\right)^2} \quad (6)$$

The total uncertainty of I_{total} ($u(I_{total})$) was calculated as:

$$u(I_{total}) = \sqrt{\sum_{i=0}^{n}\left(Pu_{surface\ activity_i} \times \sqrt{\left(\frac{u(A_i)}{A_i}\right)^2 + \left(\frac{u(DBD_i)}{DBD_i}\right)^2 + \left(\frac{u(D)}{D}\right)^2}\right)^2} \quad (7)$$

where an error of 7% ($u(DBD_i)/DBD_i$=0.07) assigned for each density measurement. The uncertainty in the $FF_{fraction}$ was calculated as:

https://doi.org/10.5194/egusphere-2026-3019
Preprint. Discussion started: 11 June 2026

$$u\left(FF_{fraction}\right) = FF_{fraction} \times \sqrt{\left(\frac{u\left(\frac{240Pu}{239Pu}_{i}\right)}{\frac{240Pu}{239Pu}_{i} - \frac{240Pu}{239Pu}_{GF}}\right)^2 + \left(\frac{u\left(\frac{240Pu}{239Pu}_{FF}\right)}{\frac{240Pu}{239Pu}_{FF} - \frac{240Pu}{239Pu}_{GF}}\right)^2 + \left(\frac{\left(\frac{240Pu}{239Pu}_{i} - \frac{240Pu}{239Pu}_{FF}\right) \times u\left(\frac{240Pu}{239Pu}_{GF}\right)}{\left(\frac{240Pu}{239Pu}_{i} - \frac{240Pu}{239Pu}_{GF}\right) \times \left(\frac{240Pu}{239Pu}_{FF} - \frac{240Pu}{239Pu}_{GF}\right)}\right)^2}$$

3 Results and discussion

3.1 $^{240}Pu/^{239}Pu$ pattern and $^{239+240}Pu$ activity peak from French fallout

The profiles of the ^{137}Cs and $^{239+240}Pu$ activity concentrations broadly overlapped in all cores (**Fig. 2**). ^{137}Cs activities typically showed a broad depth distribution ("broad peak" or "staircase-like" distribution), whereas the $^{239+240}Pu$ activity profiles often showed one or two discrete peaks. In lakes **BAR, LAJA** and **ROCA**, the depths of maximum ^{137}Cs and $^{239+240}Pu$ activities coincided (**Table 1;** BAR: **Fig. S4**). In **NAT** and **RDB**, the $^{239+240}Pu$ maximum was slightly shifted by 0.5 and 2 cm above the ^{137}Cs maximum but still fell within the broader ^{137}Cs peak (NAT: **Fig. S4**). In contrast, the $^{239+240}Pu$ maximum in **EST**, **MEL** and **NLU** occurred 8, 3 and 5 cm respectively, above the ^{137}Cs peak, forming a distinct peak, while the secondary $^{239+240}Pu$ did align with the ^{137}Cs maximum (**Table 1**, MEL: **Fig. S4**). The number of discrete $^{239+240}Pu$ peaks can be primarily explained by the sampling resolution relative to the sedimentation rate and sediment dynamics. Additionally, although ^{137}Cs is known to be mobile, it is unlikely that the depth of its maximum activity concentration has shifted significantly.

The $^{210}Pb_{ex}$-based chronology, verified by the ^{137}Cs peak, allowed us to quantify the sedimentation rates across all lakes and estimate the age of sediment deposition using the CFCS model (**Fig S6-S13**). The CRS model was applied only to **BAR (Fig. S9)** and **NLU** (**Fig. S10**), where the latter showed very low ^{137}Cs (~1 $Bq \cdot kg^{-1}$), preventing the precise identification of the ^{137}Cs peak. The $^{239+240}Pu$ data served only as an indicator to help decide between the two models for **MEL** (**Fig. S8**).

The highest sedimentation rates were estimated for **EST** (1.15±0.07 $cm.yr^{-1}$, R^2=0.88) and **RDB** (0.61±0.03 $cm.yr^{-1}$, R^2=0.96). For **MEL**, **BAR**, **NLU**, **ROCA**, **LAJA** and **NAT**, sedimentation rates were equal to or less than 0.2 $cm.yr^{-1}$, though some cores showed increases above this value in the shallower, more recent sections. The previously published **RDB** $^{210}Pb_{ex}$ based age-depth model was verified using $^{239+240}Pu$ activity and the $^{240}Pu/^{239}Pu$ atom ratio (Bardelle et al., 2025). However, its specific $^{240}Pu/^{239}Pu$ atom ratio pattern was not discussed. Depending on the sampling resolution (**Table S1**), each sample represented approximately two to ten years of deposition, with the best temporal resolution being ~2 years per sample for **EST** and **RDB**.

For the group of lakes **BAR**, **LAJA** and **ROCA** (where Cs and Pu peaks coincided), the Pu isotopic signature at the activity peaks fell within the global fallout (GF) range, with $^{240}Pu/^{239}Pu$ atom ratios between 0.165 (±0.026) and 0.193 (±0.011) (**Table 1**)**.** The $^{240}Pu/^{239}Pu$ atom ratio at the ^{137}Cs peak for **RDB** and **NAT** was partly associated with GF, but

https://doi.org/10.5194/egusphere-2026-3019
Preprint. Discussion started: 11 June 2026

the maximum Pu peak showed lower $^{240}Pu/^{239}Pu$ atom ratio of 0.082 (±0.002) and 0.132 (±0.006) respectively, indicating a mix of GF and FF contributions. In **BAR**, **LAJA**, and **RDB**, a secondary and shallower $^{239+240}Pu$ peak, observed at the extremities of the ^{137}Cs peak, had significantly lower $^{240}Pu/^{239}Pu$ atom ratios (0.059–0.074) compared to their maximum Pu peak (**Table 1, Fig. 2**). This suggests a predominant FF contribution, with a minor contribution from GF associated with this secondary Pu peak. For **RDB**, the secondary shallower Pu peak was associated with $^{240}Pu/^{239}Pu$ atom ratios of 0.075 (±0.003) and 0.069 (±0.003), consistent with previous findings by Chaboche et al. (2022). **ROCA** and **NAT** were specific in that their lowest $^{240}Pu/^{239}Pu$ atom ratio was not associated with a Pu peak but rather with declining Pu activity at the Pu peak. However, the higher $^{240}Pu/^{239}Pu$ atom ratios, observed at greater depth, might be linked to a secondary pre-Cs Pu peak (**Fig. 2** and **Table 1**).

For the group of lakes **EST**, **MEL** and **NLU,** the maximum Pu peak (which does not match the ^{137}Cs peak) presented low $^{240}Pu/^{239}Pu$ atomic ratio (0.031-0.066), within the same range as the secondary Pu peak of the previous group (**Table 1**). In **EST**, this maximum Pu peak had an activity concentration, with a value four times higher than that of the secondary and deeper peak which coincides with the Cs peak. This maximum peak is associated with the lowest $^{240}Pu/^{239}Pu$ atom ratio observed among all lakes (0.031±0.001 and 0.038±0.002), indicating a fallout source exclusively attributable to French NWTs (Chiappini et al., 1996, 1999; Hrnecek et al., 2005). In **MEL** and **NLU**, the maximum Pu peak had also a low $^{240}Pu/^{239}Pu$ atom ratio of 0.066 (±0.002) and 0.053 (±0.036), respectively. When the Pu content is low, as in the case of **NLU**, a small maximum Pu peak can be identified and used as an alternative time marker to the ^{137}Cs peak (**Fig. S8**) to indicate the French nuclear testing period ($^{240}Pu/^{239}Pu$=0.053±0.036).

The differences between Pu and Cs activity concentration profiles reflect variations in fallout sources, as indicated by their associated $^{240}Pu/^{239}Pu$ atom ratios among cores, and are not solely attributable to sedimentation dynamics or post-depositional processes. As previously used to decipher fallout sources and attribute deposition periods, the $^{137}Cs/^{239+240}Pu$ activity ratio was tested against the $^{240}Pu/^{239}Pu$ atom ratio as an additional tool (**Fig. S5**), but it appears less reliable than the $^{240}Pu/^{239}Pu$ atom ratio. A lag between the source indicated by the $^{137}Cs/^{239+240}Pu$ activity peak and the $^{240}Pu/^{239}Pu$ ratio atom was observed. The $^{240}Pu/^{239}Pu$ atom ratio provides a more precise indication of the different source periods or transitions between them.

The $^{240}Pu/^{239}Pu$ atom ratios measured in lake sediments of South America are consistent with the low $^{240}Pu/^{239}Pu$ ratio of 0.11 (±0.02, n=14) measured by the Health and Safety Laboratory (HASL) in 1969-1970 for atmospheric sampling at 40°S, 70°W (Leifer and Chan, 1997). This aligns well with $^{240}Pu/^{239}Pu$ atom ratios measured in Antarctic ice layers dating back to the French test period, which dropped to 0.09 during November1969-February 1971(Koide et al., 1985), following the French thermonuclear tests of 1968 and 1970 (≥1 Mt), indicating a mix between the GF and FF contributions.

https://doi.org/10.5194/egusphere-2026-3019
Preprint. Discussion started: 11 June 2026

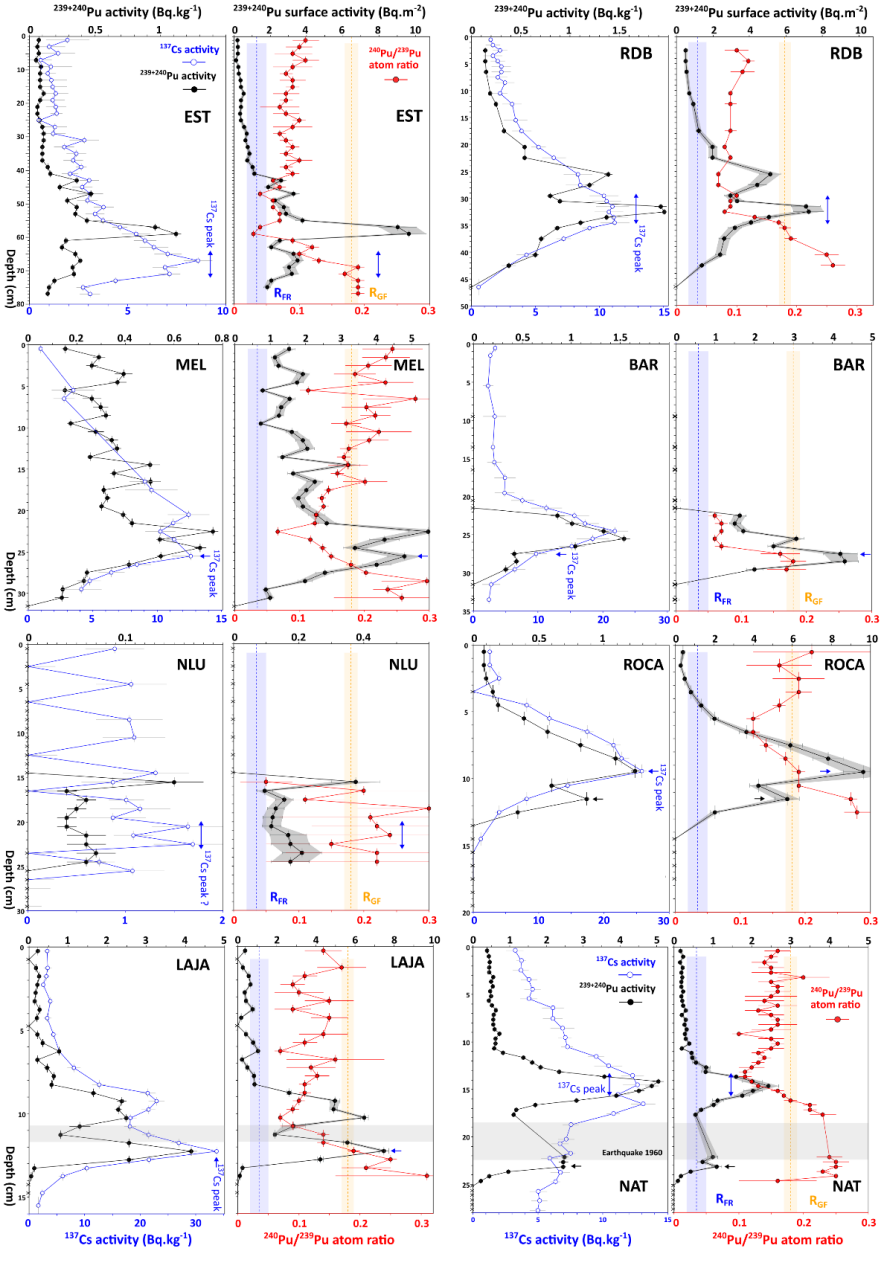

Figure 2: Depth profiles of (left) ^{137}Cs (blue) and $^{239+240}$Pu (black) activities concentrations (Bq·kg^{-1}) and of (right) $^{239+240}$Pu surface activity (black, Bq·m^{-2}) with uncertainty range (grey transparent ribbon) and the ^{240}Pu/^{239}Pu atom ratio (red) from the eight lakes in South America. Colored vertical ribbons indicate the main ^{240}Pu/^{239}Pu isotopic signatures with R_{GF} (Global Fallout ratio, 0.18±0.01) and R_{FR} (French Fallout ratio, 0.035±0.015). Grey horizontal bands mark instantaneous events, which do not represent continuous sedimentation. Note that the ^{240}Pu/^{239}Pu axis scale is consistent across all lake graphs.

Table 1: Summary of ^{137}Cs (decay-corrected to 2026) and $^{239+240}$Pu peak activities and associated ^{240}Pu/^{239}Pu atom ratio for the different lakes. The ^{137}Cs activity is expressed as ^{137}Cs surface activity (Bq·m^{-2}) for the underlined values due to changes in density for MEL, BAR and NAT (Fig.S4).

Lakes	Maximum ^{137}Cs activity peak				Maximum $^{239+240}$Pu activity peak				Secondary $^{239+240}$Pu activity peak			
	^{137}Cs activity (Bq.kg^{-1})	^{137}Cs surface activity (Bq.m^{-2})	Depth (cm)	^{240}Pu/^{239}Pu atom ratio	$^{239+240}$Pu activity (Bq.kg^{-1})	$^{239+240}$Pu surface activity (Bq.m^{-2})	Depth (cm)	^{240}Pu/^{239}Pu atom ratio	$^{239+240}$Pu activity (Bq.kg^{-1})	$^{239+240}$Pu surface activity (Bq.m^{-2})	Depth (cm)	^{240}Pu/^{239}Pu atom ratio
BAR	10.4	100	**27.5**	0.165 (±0.026)	0.4-0.4	4.2-4.3	**27.5-28.5**	0.165 -0.176 (±0.023-0.026)	1.5	3.1	25.5	0.059 (±0.003)
LAJA	34.5	61	**12.25**	0.193 (±0.011)	4.2	7.5	**12.25**	0.193 (±0.011)	2.5	6.5	10.25	0.074 (±0.003)
ROCA[1]	26	201	**9.5**	0.188 (± 0.006)	1.2	10	**9.5**	0.188 (± 0.006)	0.9	5.7	11.5	0.274 (± 0.007)
RDB	10.4-11.2	40-41	**29.5-34.5**	0.087-0.175 (±0.002-0.007)	1.9-2.0	7.2-7.2	**31.5-32.5**	0.082-0.087 (± 0.002-0.003)	1.4	5.2	25.5	0.069 (±0.003)
NAT[1]	11.2-12.7	3.8-4.5	**13.5-15.5**	0.106-0.171 (±0.008-0.004)	4.9	2.4	**14.65**	0.132 (±0.006)	2.4	1.1	23.15	0.247 (±0.010)
EST	7.2-9.0	66-80	**65-71**	0.101-0.185 (±0.005-0.008)	1.1	9-10	57-59	0.031- 0.038 (±0.001- 0.002)	0.3-0.4	3.1-3.5	**65-71**	0.101-0.185 (±0.005-0.008)
MEL	13	111.1	**25.5**	0.149 (±0.006)	0.76	5.5	22.5	0.066 (±0.002)	0.5	4.8	**25.5**	0.149 (±0.006)
NLU	1.1-1.7	3-5	**20.5-22.5**	**n.a**	0.2	0.4	15.5	0.053 (±0.036)	≤ 0.08	0.2	**21.5-24.5**	**n.a**

[1]Please note that the secondary Pu peak referred to for **NAT** and **ROCA** corresponds to a minor, potential peak at a deeper depth.

https://doi.org/10.5194/egusphere-2026-3019
Preprint. Discussion started: 11 June 2026

3.2 Improving chronologies with $^{240}Pu/^{239}Pu$ isotope ratio and $^{239+240}Pu$ activity peak

Core dating by $^{210}Pb_{ex}$ allowed us to verify the consistency between fallout sources indicated by the $^{240}Pu/^{239}Pu$ atom ratios and the deposition dates computed using the $^{210}Pb_{ex}$ chronology. With the exception of **EST** and **BAR**, high $^{240}Pu/^{239}Pu$ atom ratios (~ 0.25) were observed in the deepest sediments of **NAT**, **LAJA**, **MEL**, **ROCA** and **RDB** (**Fig. 2**). These high ratios corresponded to fallout sources deposited during the pre-moratorium period and dated to the early 1950s (**Fig. 3**). **NAT** and **ROCA** are the two lakes potentially showing a secondary deeper and smaller Pu peak preceding the ^{137}Cs peak (pre-moratorium), linked to a high $^{240}Pu/^{239}Pu$ atom ratio between 0.247 (± 0.010) and 0.274 (± 0.007) (**Fig. 2, Table 1**). In **BAR**, low Pu activities associated with high $^{240}Pu/^{239}Pu$ uncertainties prevented a clear identification of these high ratios, likely due to lower fallout deposition in this semi-arid area (**Fig. S2**). Since **EST** was only constructed during the pre-moratorium period, no fallout record is available for this period.

With increasing $^{239+240}Pu$ activity, the $^{240}Pu/^{239}Pu$ atom ratios of all lakes decreased toward values close to 0.18 during the post-moratorium period, corresponding to the $^{239+240}Pu$ peak that coincides with the ^{137}Cs peak. From the GF ratio of ~ 0.18, the $^{240}Pu/^{239}Pu$ atom ratio further decreased to values below 0.18, reaching ~ 0.14. This trend aligns with $^{240}Pu/^{239}Pu$ atom ratios measured in Antarctic ice layers dating back to the French NWTs period, where ratios ranged from 0.14 to 0.15 for March 1966 - October1968 following the first French Polynesian tests in 1966 and 1967.

The lowest $^{240}Pu/^{239}Pu$ atom ratios (<0.074), dated to the late 1960s and the early 1970s (**Fig. 3)**, correspond to the period of French atmospheric tests, particularly the high-yield thermonuclear tests conducted in 1968 and 1970 (UNSCEAR, 2000). The low Pu activity observed in between peaks of **EST** (62 cm) and **RDB** (29-31 cm) likely corresponds to periods without French atmospheric tests, such as the 20-month gap in NWTs between 1968 and 1970, or seasonal NWTs pauses during austral summer. Since each sample layer represents approximately two years of deposition in both cases, these testing gaps might be reflected in the low Pu activity concentrations.

The main ^{137}Cs peak is attributed to a combination of residual global fallout from high-altitude stratospheric tests and early French atmospheric tests in the mid-1960s. These tests were characterized by intermediate yields (28–125 kt) and detonation heights ranging from tens to hundreds of meters (up to 1200 m), which potentially favored the significant production and widespread transport of volatile fission products like ^{137}Cs. This interpretation is supported by air fallout data from Buenos Aires (**Fig. S2**), which recorded prolonged peaks of short-lived radionuclides in September–October 1966, confirming the regional arrival of the French plume (Tassano et al., 2025).

For Pu, the more recent peak, which represents either the maximum Pu peak or a secondary Pu peak during the late 1960s and early 1970s, coincides with tests dominated by high-yield thermonuclear devices (e.g., Canopus, 2.6 Mt, 1968; Dragon, 945 kt, 1970; and Rhea, 955 kt, 1971). These tests were conducted at variable altitudes (e.g., 220-700 m) mainly using plane as drop mode and exhibited significantly higher yields compared to earlier fission-based tests (1966-1967). The thermonuclear tests may have produced fallout richer in particulate Pu and poorer in ^{137}Cs, likely due to differences in device design, test yields, and radionuclide partitioning. This shift is well reflected in the sediment profiles, where Pu peaks are often decoupled from ^{137}Cs maxima and exhibit lower $^{240}Pu/^{239}Pu$ ratios (0.031–0.074), indicative of a dominant FF contribution.

https://doi.org/10.5194/egusphere-2026-3019
Preprint. Discussion started: 11 June 2026

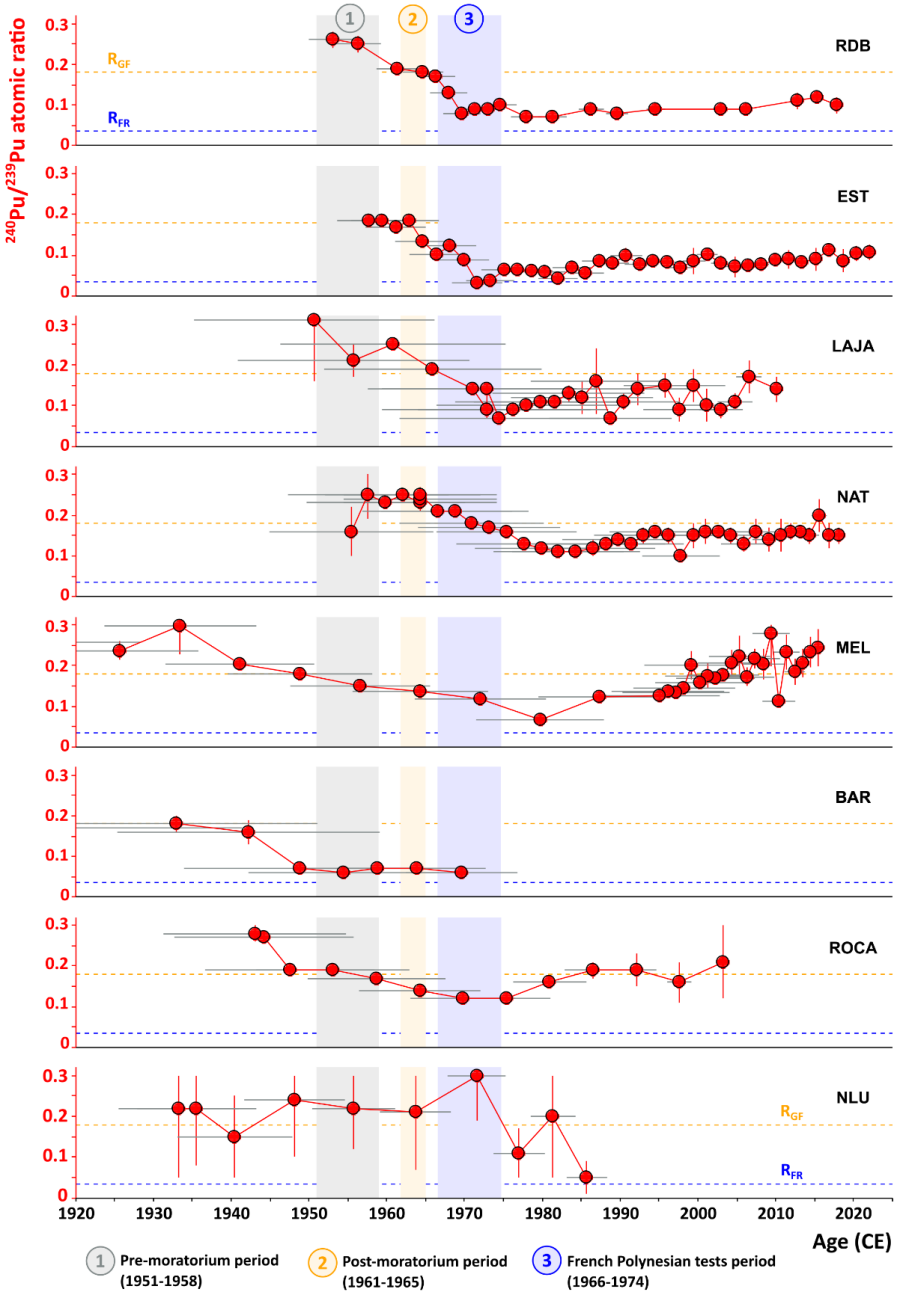

Figure 3: Compilation of the ^{240}Pu/^{239}Pu atom ratio over time. Ages were independently determined from the ^{210}Pb$_{ex}$ chronology, validated by the location of the ^{137}Cs peak. Colored lines indicate the main ^{240}Pu/^{239}Pu isotopic signatures: Global Fallout (R_{GF} = 0.18, in yellow) and French Fallout (R_{FR} = 0.035, in blue).

https://doi.org/10.5194/egusphere-2026-3019
Preprint. Discussion started: 11 June 2026

The more recent Pu peak, associated with declining ^{137}Cs activity (**Fig. 2**), provided a second time marker approximately four to six years after the ^{137}Cs activity peak (assigned to 1964-1965, depending on sampling resolution). These results support the chronological reconstruction of NWTs in the SH and validate the temporal patterns of ^{240}Pu/^{239}Pu ratios initially reported in Antarctica (Koide et al., 1985). The shallower Pu peak can therefore serve as an alternative time marker for the 1968-1971 period, coinciding with the French thermonuclear tests. Together with the ^{240}Pu/^{239}Pu atom ratio pattern, it provides control points for the entire period of nuclear weapon tests (1952–1974).

3.3 Spatial disparities of Pu deposition in the 32-52°S latitudinal band and French fallout contribution

To compare $^{239+240}$Pu deposition across the 32-52°S latitudinal band, Pu fluxes were calculated for all lakes (**Fig. 4**). As shown in **Fig. 3**, most of the age-depth model calculated from the ^{210}Pb$_{ex}$ and verified with ^{137}Cs activities (**BAR, MEL, LAJA, NLU, NAT, ROCA; Fig S8-S13**) provided relatively high age uncertainty of sediment deposition during the last century. In contrast, the ^{240}Pu/^{239}Pu atom ratio, associated with specific nuclear test sources or their mixing across different periods, proved to provide a more reliable time marker for sediment deposition. During the pre-moratorium period (with ^{240}Pu/^{239}Pu ratio >0.20), fluxes remained below 1 Bq·m^{-2}.yr^{-1}, except for **RDB**. In the post-moratorium period (^{240}Pu/^{239}Pu ratio ~ 0.18) fluxes differed between **LAJA**, **EST** and **RDB** (>1 Bq·m^{-2}.yr^{-1}) and **MEL**, **NAT** and **BAR** (<1 Bq·m^{-2}.yr^{-1}). For **NLU**, high uncertainties in the ^{240}Pu/^{239}Pu atom ratios prevented flux reconstruction (**Fig. 2-3**), except for its minor Pu peak (eq. 0.1 Bq·m^{-2}.yr^{-1}), which can be associated with the French nuclear tests (**Fig. 4**).

Pu fluxes generally increased as ^{240}Pu/^{239}Pu atom ratio decreased (^{240}Pu/^{239}Pu<0.14), with **EST** and **RDB** fluxes showing a strong flux increase (>4 Bq·m^{-2}.yr^{-1}) associated with low isotopes ratios, thus indicating predominant FF contribution. In contrast, **BAR** and **MEL** were impacted by generally low fluxes (<1 Bq·m^{-2}.yr^{-1}, **Fig. 4**), despite being located at similar latitudes to **EST** and **RDB** within the humid Pampa biome. Very likely, this can be related to the lower precipitation rates at **BAR** and **MEL**, which received on average only half the annual precipitation compared to **RDB** and **EST** (**Table S1**). With an equivalent ^{240}Pu/^{239}Pu atom ratio, **LAJA** and **NAT,** located on the wetter western flank of the southern Andes in Chile (**Fig. S1**), showed higher Pu fluxes than **BAR, MEL** and **NLU** although lower fluxes than **RDB** and **EST**, likely due to their more southern position. Between **LAJA** and **NAT**, the more northerly **LAJA** showed the highest fluxes, further illustrating the N-S trend. **NLU**, located in the drier Patagonian steppe, showed the lowest precipitation regime among all studied sites (**Fig. S1**), which likely explained the very low ^{137}Cs and Pu deposition. Precipitation is likely the limiting factor controlling the lower Pu deposition in **BAR**, **MEL** and **NLU**, despite similar ^{240}Pu/^{239}Pu atom ratio patterns. This comparison indicates that our sites in Uruguay, due to their proximity to the latitude of injection of the French Polynesian test sites (**Fig. 1**) and its relatively high annual precipitation, has received quantitatively more FF within the 32-52ºS latitudinal band.

ROCA showed an opposite pattern, with higher Pu flux associated with the pre-moratorium period (up to 3.5 Bq·m^{-2}.yr^{-1}) and lower fluxes (< 1 Bq·m^{-2}.yr^{-1}) during the French tests period (lowest ^{240}Pu/^{239}Pu). This pattern aligns well with the Antarctic ice core records (Koide et al., 1985), where pre-moratorium Pu deposition was more

https://doi.org/10.5194/egusphere-2026-3019
Preprint. Discussion started: 11 June 2026

pronounced at southern latitudes, reflecting greater influence from the Pacific Proving Ground tests (**Fig.1**) and a reduced FF contribution.

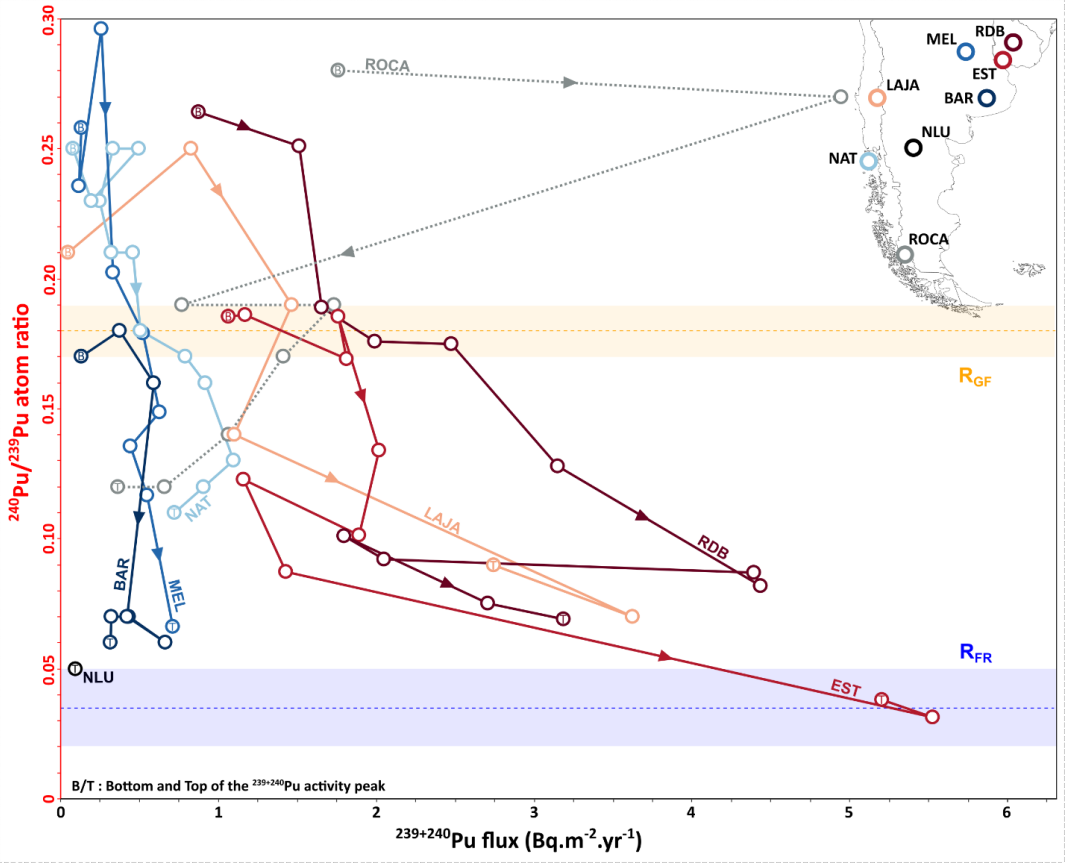

Figure 4: $^{239+240}$Pu fluxes (Bq·m^{-2}.yr^{-1}) versus the ^{240}Pu/^{239}Pu atom ratio for sediment layers within the $^{239+240}$Pu activity peak of each lake. Point B (bottom) represents the deepest sediment of the Pu peak, point T (top) the shallowest, and the arrow indicates the direction of sedimentation. The lake color gradient ranges from dark red (highest flux) to light blue (lowest flux).

The $^{239+240}$Pu peak lake inventories (I_{peak}) were calculated and compared with total $^{239+240}$Pu inventories and reference inventories derived from nearby soils or soils collected at the same latitude (**Fig. S1**). I_{peak} ranged from 1.7 to 74.0 Bq·m^{-2} (**Table S2**), which in most cases was higher than median latitudinal band inventories (**Fig. 5**). **EST** and **RDB** presented the highest I_{peak} while **NAT**, **NLU** and **BAR** showed the lowest calculated inventories. The contribution of the FF, estimated from the $^{239+240}$Pu inventories of the layers deposited during the period of nuclear weapon testing, ranged from 13 (±7%) to 52% (±13%) and allows comparison of the relative magnitude of FF within lakes. **ROCA** and **NAT** showed the smallest contribution of FF (~15%). This minor fraction is consistent with the

https://doi.org/10.5194/egusphere-2026-3019
Preprint. Discussion started: 11 June 2026

absence of a measurable FF fraction in the Punta Arenas reference soil and a similar fraction in the Puerto Montt reference soil, located less than 200 km north of **NAT** (**Fig. 5**). The two southernmost lakes investigated agreed with the low FF deposition within the 40-50°S latitudinal band (Buesseler, 1997; Koide et al., 1985). The FF fraction for **NLU** could not be calculated due to high uncertainties in the $^{240}Pu/^{239}Pu$ atom ratio. **EST**, **RDB, LAJA**, **MEL** and **BAR** have the largest FF fraction calculated within I_{peak} (≥30%), confirming the highest FF fraction within the 30-40°S latitude band (**Table 2**).

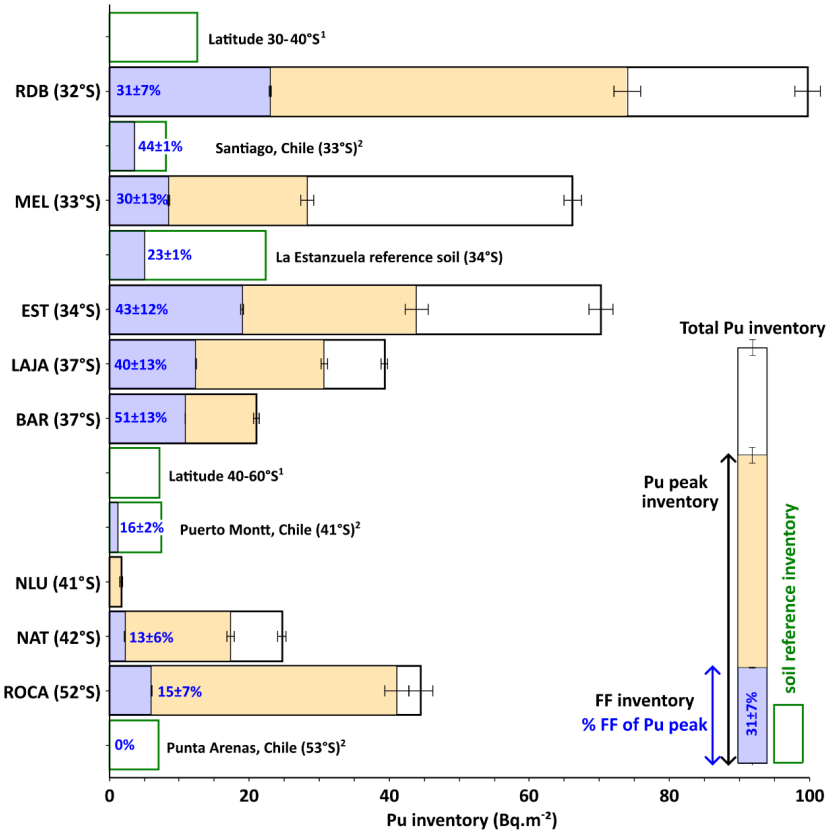

[1]median in South America, Dicen et al. 2025 [2] Krey et al. 1976, Kelley et al. 1999: Punta Arenas $^{240}Pu/^{239}Pu = 0.2045 \pm 0.005$ Puerto Montt $^{240}Pu/^{239}Pu = 0.153 \pm 0.001$ Santiago $^{240}Pu/^{239}Pu = 0.116 \pm 0.002$.

Figure 5: Total Pu and Pu Peak Inventories (Bq.m^{-2}) with French Fallout (FF) Fraction (%) and Soil Reference Inventories.

The higher deposition of FF in Uruguay is also reflected in the low $^{240}Pu/^{239}Pu$ atom ratios measured in recently deposited sediments (post-tests period), where the average did not exceed 0.10 for **EST** and **RDB**, indicating a recent FF contribution between 30-50% (**Fig. 3**). This suggests that the total abundance of Pu fallout from French tests in Uruguayan soils was not only higher than in other regions but also results in a persistent FF signature in soil particles, which are eroded and transported to the lake basins. This interpretation is the most likely explanation for the continued

https://doi.org/10.5194/egusphere-2026-3019
Preprint. Discussion started: 11 June 2026

presence of mixed French and global fallout Pu signatures in sediments more than 50 years after the end of atmospheric nuclear weapons testing.

Conclusions

This study provided a revised interpretation of ^{137}Cs and $^{239+240}$Pu fallout in the southern South America region, highlighting that artificial radionuclide deposition is not restricted to a single 1964-1965 peak. Instead, a more recent Pu peak, associated with declining ^{137}Cs activity, can served as an additional time marker for 1968-1971, coinciding with French thermonuclear tests and occurring 4–6 years after the ^{137}Cs maximum.

Additionally, this work provided evidence for the revaluation of existing ^{137}Cs conversion models (e.g., for soil erosion assessment), as radionuclide fallout may not be limited to the Global fallout fraction alone. The temporal reconstruction of $^{239+240}$Pu deposition explained the highest FF deposition within the 30-40°S latitudinal band, influenced by precipitation and the proximity to the latitude at which the French Polynesian tests were conducted (22°S). The ^{240}Pu/^{239}Pu atom ratio allowed the identification of specific fallout sources or their mixing, linking them to three distinct historical testing periods (pre-moratorium, post-moratorium and the French tests periods), and thereby contributes refining age-depth models for more accurate environmental reconstructions during the Anthropocene.

Appendix A

No Appendix A

Code and data availability

The data file will be put online during the revision process- Link to zenodo

Supplement link

The supplementary information data are presented in the supplementary information word file.

Author contribution

Conceptualization: the AVATAR project was conceptualized by Olivier Evrard (OE), Christine Alewell (CA) and Pierre Sabatier (PS). The evolution of overarching research goals and aims leading to this publication were led by Floriane Guillevic (FG) and Renaldo Gastineau (RG) with regular support of the co-authors. **Data curation**: FG and RG were responsible for data management. **Funding acquisition**: OE, CA and PS led the acquisition of financial support for the project. **Formal analysis and Investigation** Amaury Bardelle (AB), Pierre-Alexis Chaboche (PC), Anthony Foucher (AF) were involved in the **RDB** core collection, core analysis and gamma measurement. Romina Achaga (RA), Ana Carolina Ruiz-Fernández (ARF), Joan-Albert Sanchez-Cabeza (JSC) were involved in the **MEL**

https://doi.org/10.5194/egusphere-2026-3019
Preprint. Discussion started: 11 June 2026

and **BAR** cores collection, core analysis and gamma measurement. For **NLU**, RA was involved in the core collection and core analysis. Marcos Tassano (MT), Mirel Cabrera (MC), Juan A. Quicke (JQ) , Guillermo Chalar (GC), were involved in the **EST** core collection, core analysis and gamma measurement. Maarten Van Daele (MVD) was involved in **LAJA** core collection, core analysis. Valentina Moreno-Allende (VMA), Jasper Moernaut (JM), were involved in the **NAT** core collection and core analysis. For **ROCA**, Torsten Haberzettl (TH) was involved in the core collection and core analysis. RG performed the rest of the computation of gamma results for age-depth models. José A. Corcho Alvarado (JCA), Stefan Röllin (SR), Hans Sahli (HS) managed half of the Pu extraction and all Pu measurements. The other half of the Pu extraction was performed by FG with the participation and support of Judith Kobler (JK), Gerald Dicen (GD). FG conducted the formal analysis of plutonium isotopes results **Validation**: FG, RG, PS, JCA and SR were responsible for data validation , and all co-authors have verified related information on the core they have collected and/or investigated. **Visualization:** FG and RG. **Writing (original draft preparation):** FG prepared the manuscript with initial contribution of RG, GD, OE, PS, JCA and CA across different versions leading to the original draft. The final version was verified and edited by all the co-authors. **Writing (review and editing):** need to be updated.

Competing interests

The authors declared no competing interests.

Disclaimer

No disclaimer.

Acknowledgements

The authors would like to acknowledge the contribution of Alice Mollard, a technical engineer at EDYTEM, to the gamma measurements.

Financial support

The AVATAR project is funded by the Swiss National Science Foundation (SNSF; grant no. 212886) and the French National Research Agency (ANR; grant no. ANR-22-CE93-0001). J. Moernaut and V. Moreno-Allende acknowledge financial support by the Austrian Science Fund (FWF) [10.55776/P34504].

References

https://doi.org/10.5194/egusphere-2026-3019
Preprint. Discussion started: 11 June 2026

Achaga, R., Gogorza, C., Irurzun, M. A., Goguitchaichvili, A., Mestelán, S., Ruiz Fernández, A. C., Sánchez Cabeza, J. A., Sánchez Bettucci, L., Sinito, A., Morales, J., and Martínez, D.: Monitoring the environmental evolution and its relationship with anthropogenic activities using magnetic and geochemical proxies on Lake Melincué sediments, J. South Am. Earth Sci., 116, 103827, https://doi.org/10.1016/j.jsames.2022.103827, 2022.

Appleby, P. G. and Oldfield, F.: The calculation of lead-210 dates assuming a constant rate of supply of unsupported 210Pb to the sediment, CATENA, 5, 1–8, https://doi.org/10.1016/S0341-8162(78)80002-2, 1978.

Bardelle, A., Gastineau, R., Guillevic, F., Foucher, A., Chaboche, P.-A., Corcho-Alvarado, J. A., Röllin, S., Chalar, G., Sabatier, P., Tassano, M., Cottin, N., Vandromme, R., Cerdan, O., Alewell, C., and Evrard, O.: The hidden consequences of agricultural development: Soil degradation and pesticide contamination in the South American Pampa, Sci. Total Environ., 1002, 180584, https://doi.org/10.1016/j.scitotenv.2025.180584, 2025.

Barra, R., Cisternas, M., Urrutia, R., Pozo, K., Pacheco, P., Parra, O., and Focardi, S.: First report on chlorinated pesticide deposition in a sediment core from a small lake in central Chile, Chemosphere, 45, 749–757, https://doi.org/10.1016/S0045-6535(01)00146-1, 2001.

Bouisset, P., Nohl, M., Bouville, A., and Leclerc, G.: Inventory and vertical distribution of 137Cs, 239+240Pu and 238Pu in soil from Raivavae and Hiva Oa, two French Polynesian islands in the southern hemisphere, J. Environ. Radioact., 183, 82–93, https://doi.org/10.1016/j.jenvrad.2017.12.017, 2018.

Bouisset, P., Nohl, M., Cossonnet, C., Boulet, B., Thomas, S., Cariou, N., and Salaun, G.: Contribution of close-in fallout from the French atmospheric tests in inventories of 137Cs, 241Am and plutonium (238, 239, 240) in Gambier Islands (French Polynesia) – Signatures of stratospheric fallout in the Southern Hemisphere, J. Environ. Radioact., 235–236, 106624, https://doi.org/10.1016/j.jenvrad.2021.106624, 2021.

Browne, E.: Nuclear Data Sheets for A = 235,239, Nucl. Data Sheets, 98, 665–800, https://doi.org/10.1006/ndsh.2003.0005, 2003.

Browne, E. and Tuli, J. K.: Nuclear Data Sheets for A = 236, Nucl. Data Sheets, 107, 2649–2714, https://doi.org/10.1016/j.nds.2006.09.002, 2006.

Bruel, R. and Sabatier, P.: serac: an R package for ShortlivEd RAdionuclide chronology of recent sediment cores, J. Environ. Radioact., 225, 106449, https://doi.org/10.1016/j.jenvrad.2020.106449, 2020.

Buesseler, K. O.: The isotopic signature of fallout plutonium in the North Pacific, J. Environ. Radioact., 36, 69–83, https://doi.org/10.1016/S0265-931X(96)00071-9, 1997.

Chaboche, P.-A., Pointurier, F., Sabatier, P., Foucher, A., Tiecher, T., Minella, J. P. G., Tassano, M., Hubert, A., Morera, S., Guédron, S., Ardois, C., Boulet, B., Cossonnet, C., Cabral, P., Cabrera, M., Chalar, G., and Evrard, O.: 240Pu/239Pu signatures allow refining the chronology of radionuclide fallout in South America, Sci. Total Environ., 843, 156943, https://doi.org/10.1016/j.scitotenv.2022.156943, 2022.

Chamizo, E., García-León, M., Peruchena, J. I., Cereceda, F., Vidal, V., Pinilla, E., and Miró, C.: Presence of plutonium isotopes, 239Pu and 240Pu, in soils from Chile, Nucl. Instrum. Methods Phys. Res. Sect. B Beam Interact. Mater. At., 269, 3163–3166, https://doi.org/10.1016/j.nimb.2011.04.021, 2011.

Chiappini, R., Taillade, J.-M., and Brébion, S.: Development of a high-sensitivity inductively coupled plasma mass spectrometer for actinide measurement in the femtogram range, J. Anal. At. Spectrom., 11, 497–503, https://doi.org/10.1039/JA9961100497, 1996.

Chiappini, R., Pointurier, F., Millies-Lacroix, J. C., Lepetit, G., and Hemet, P.: 240Pu/239Pu isotopic ratios and 239+240Pu total measurements in surface and deep waters around Mururoa and Fangataufa atolls compared with Rangiroa atoll (French Polynesia), Sci. Total Environ., 237–238, 269–276, https://doi.org/10.1016/S0048-9697(99)00141-2, 1999.

https://doi.org/10.5194/egusphere-2026-3019
Preprint. Discussion started: 11 June 2026

Child, D. P. and Hotchkis, M. A. C.: Plutonium and uranium contamination in soils from former nuclear weapon test sites in Australia, Nucl. Instrum. Methods Phys. Res. Sect. B Beam Interact. Mater. At., 294, 642–646, https://doi.org/10.1016/j.nimb.2012.05.018, 2013.

Dicen, G., Guillevic, F., Gupta, S., Chaboche, P.-A., Meusburger, K., Sabatier, P., Evrard, O., and Alewell, C.: Distribution and sources of fallout^{137} Cs and$^{239+240}$ Pu in Equatorial and Southern Hemisphere reference soils, https://doi.org/10.5194/essd-2024-509, 11 November 2024.

Foucher, A., Chaboche, P.-A., Sabatier, P., and Evrard, O.: A worldwide meta-analysis (1977–2020) of sediment core dating using fallout radionuclides including ^{137}Cs and ^{210}Pb$_{xs}$, Earth Syst. Sci. Data, 13, 4951–4966, https://doi.org/10.5194/essd-13-4951-2021, 2021.

Foucher, A., Tassano, M., Chaboche, P.-A., Chalar, G., Cabrera, M., Gonzalez, J., Cabral, P., Simon, A.-C., Agelou, M., Ramon, R., Tiecher, T., and Evrard, O.: Inexorable land degradation due to agriculture expansion in South American Pampa, Nat. Sustain., 6, 662–670, https://doi.org/10.1038/s41893-023-01074-z, 2023.

Guevara, S., Rizzo, A., Sanchez, R., and Arribere, M.: Pb-210 fluxes in sediment layers sampled from Northern Patagonia lakes, J. Radioanal. Nucl. Chem., 258, 583–595, 2003.

Guillevic, F., Sabatier, P., Dicen, G., Aggarwal, P., Foucher, A., Evrard, O., and Alewell, C.: Assessing the artificial radionuclide Cesium-137 spatial distribution in the Southern Hemisphere from lake sediment records, J. Environ. Radioact., 293, 107906, https://doi.org/10.1016/j.jenvrad.2026.107906, 2026.

Hancock, G. J., Leslie, C., Everett, S. E., Tims, S. G., Brunskill, G. J., and Haese, R.: Plutonium as a chronomarker in Australian and New Zealand sediments: a comparison with 137Cs, J. Environ. Radioact., 102, 919–929, https://doi.org/10.1016/j.jenvrad.2009.09.008, 2011.

Hancock, G. J., Tims, S. G., Fifield, L. K., and Webster, I. T.: The release and persistence of radioactive anthropogenic nuclides, Geol. Soc. Lond. Spec. Publ., 395, 265–281, https://doi.org/10.1144/SP395.15, 2014.

Hrnecek, E., Steier, P., and Wallner, A.: Determination of plutonium in environmental samples by AMS and alpha spectrometry, Appl. Radiat. Isot., 63, 633–638, https://doi.org/10.1016/j.apradiso.2005.05.012, 2005.

Kelley, J. M., Bond, L. A., and Beasley, T. M.: Global distribution of Pu isotopes and 237Np, Sci. Total Environ., 237–238, 483–500, https://doi.org/10.1016/S0048-9697(99)00160-6, 1999.

Ketterer, M. E. and Szechenyi, S. C.: Determination of plutonium and other transuranic elements by inductively coupled plasma mass spectrometry: A historical perspective and new frontiers in the environmental sciences, Spectrochim. Acta Part B At. Spectrosc., 63, 719–737, https://doi.org/10.1016/j.sab.2008.04.018, 2008.

Ketterer, M. E., Hafer, K. M., and Mietelski, J. W.: Resolving Chernobyl vs. global fallout contributions in soils from Poland using Plutonium atom ratios measured by inductively coupled plasma mass spectrometry, J. Environ. Radioact., 73, 183–201, https://doi.org/10.1016/j.jenvrad.2003.09.001, 2004.

Koide, M., Bertine, K. K., Chow, T. J., and Goldberg, E. D.: The240Pu239Pu ratio, a potential geochronometer, Earth Planet. Sci. Lett., 72, 1–8, https://doi.org/10.1016/0012-821X(85)90112-8, 1985.

Krey, P. W., Hardy, E. P., Pachucki, C., Rourke, F., Coluzza, J., and Benson, W. K.: Mass isotopic composition of global fall-out plutonium in soil, in: Transuranium nuclides in the environment, 1976.

Leifer, R. and Chan, N.: The Environmental Measurements Laboratory's Stratospheric Radionuclide (RANDAB) and Trace Gas (TRACDAB) Databases, 1997.

Ministère de la défense: La Dimension Radiologique des Essais Nucléaires Français en Polynésie - À l'épreuve des faits, Ministère de la défense, 2006.

https://doi.org/10.5194/egusphere-2026-3019
Preprint. Discussion started: 11 June 2026

Mougeot, X., Dulieu, C., Huang, X., Kellett, M., Leblond, S., and Wang, B.: Evaluations of the decay data of 137mBa, 137Cs, 151Sm and 225Ac from the Decay Data Evaluation Project (DDEP) – 2023, Metrologia, 62, 029002, https://doi.org/10.1088/1681-7575/adb9de, 2025.

R Core Team: R: A language and environment for statistical computing., 2022.

Reyss, J.-L., Schmidt, S., Legeleux, F., and Bonté, P.: Large, low background well-type detectors for measurements of environmental radioactivity, Nucl. Instrum. Methods Phys. Res. Sect. Accel. Spectrometers Detect. Assoc. Equip., 357, 391–397, https://doi.org/10.1016/0168-9002(95)00021-6, 1995.

Röllin, S., Sahli, H., Holzer, R., Astner, M., and Burger, M.: PU and NP analysis of soil and sediment samples with ICP-MS, Appl. Radiat. Isot., 67, 821–827, https://doi.org/10.1016/j.apradiso.2009.01.041, 2009.

Röllin, S., Corcho-Alvarado, J. A., Sahli, H., Putyrskaya, V., and Klemt, E.: High-resolution records of cesium, plutonium, americium, and uranium isotopes in sediment cores from Swiss lakes, Environ. Sci. Pollut. Res., 29, 85777–85788, https://doi.org/10.1007/s11356-022-20785-y, 2022.

Rougerie, F. and Rancher, J.: The Polynesian south ocean: Features and circulation, Mar. Pollut. Bull., 29, 14–25, https://doi.org/10.1016/0025-326X(94)90421-9, 1994.

Sahli, H., Röllin, S., Putyrskaya, V., Klemt, E., Balsiger, B., Burger, M., and Corcho Alvarado, J. A.: A procedure for the sequential determination of radionuclides in soil and sediment samples, J. Radioanal. Nucl. Chem., 314, 2209–2218, https://doi.org/10.1007/s10967-017-5621-3, 2017.

Salmani-Ghabeshi, S., Chamizo, E., Christl, M., Miró, C., Pinilla-Gil, E., and Cereceda-Balic, F.: Presence of 236U and 239,240Pu in soils from Southern Hemisphere, J. Environ. Radioact., 192, 478–484, https://doi.org/10.1016/j.jenvrad.2018.08.003, 2018.

Tassano, M., Cabral, P., and Cabrera, M.: Inventario de cesio-137 y plomo-210 en suelos de referencia del centro-oeste de Uruguay:: base para estudios de erosión y vigilancia radiológica, INNOTEC, e682–e682, https://doi.org/10.26461/29.06, 2025.

UNSCEAR: SOURCES AND EFFECTS OF IONIZING RADIATION - VOLUME 1 : SOURCES, United Nations, New York, 2000.

Zalles, V., Hansen, M. C., Potapov, P. V., Parker, D., Stehman, S. V., Pickens, A. H., Parente, L. L., Ferreira, L. G., Song, X.-P., Hernandez-Serna, A., and Kommareddy, I.: Rapid expansion of human impact on natural land in South America since 1985, Sci. Adv., 7, eabg1620, https://doi.org/10.1126/sciadv.abg1620, 2021.

Zeileis, A. and Grothendieck, G.: zoo: S3 Infrastructure for Regular and Irregular Time Series, J. Stat. Softw., 14, 1–27, https://doi.org/10.18637/jss.v014.i06, 2005.